

REPORT DOCUMENTATION PAGE			Form Approved OMB NO. 0704-0188		
<p>The public reporting burden for this collection of information is estimated to average 1 hour per response, including the time for reviewing instructions, searching existing data sources, gathering and maintaining the data needed, and completing and reviewing the collection of information. Send comments regarding this burden estimate or any other aspect of this collection of information, including suggestions for reducing this burden, to Washington Headquarters Services, Directorate for Information Operations and Reports, 1215 Jefferson Davis Highway, Suite 1204, Arlington VA, 22202-4302. Respondents should be aware that notwithstanding any other provision of law, no person shall be subject to any penalty for failing to comply with a collection of information if it does not display a currently valid OMB control number.</p> <p>PLEASE DO NOT RETURN YOUR FORM TO THE ABOVE ADDRESS.</p>					
1. REPORT DATE (DD-MM-YYYY) 13-09-2017		2. REPORT TYPE Final Report		3. DATES COVERED (From - To) 1-Oct-2011 - 30-Jun-2017	
4. TITLE AND SUBTITLE Final Report: Flexoelectricity in Nanostructures: Theory, Nanofabrication and Characterization			5a. CONTRACT NUMBER W911NF-11-1-0516		
			5b. GRANT NUMBER		
			5c. PROGRAM ELEMENT NUMBER 611102		
6. AUTHORS			5d. PROJECT NUMBER		
			5e. TASK NUMBER		
			5f. WORK UNIT NUMBER		
7. PERFORMING ORGANIZATION NAMES AND ADDRESSES North Carolina State University 2701 Sullivan Drive Admin Srvcs III, Box 7514 Raleigh, NC 27695 -7514			8. PERFORMING ORGANIZATION REPORT NUMBER		
9. SPONSORING/MONITORING AGENCY NAME(S) AND ADDRESS (ES) U.S. Army Research Office P.O. Box 12211 Research Triangle Park, NC 27709-2211			10. SPONSOR/MONITOR'S ACRONYM(S) ARO		
			11. SPONSOR/MONITOR'S REPORT NUMBER(S) 58405-EL.19		
12. DISTRIBUTION AVAILABILITY STATEMENT Approved for public release; distribution is unlimited.					
13. SUPPLEMENTARY NOTES The views, opinions and/or findings contained in this report are those of the author(s) and should not be construed as an official Department of the Army position, policy or decision, unless so designated by other documentation.					
14. ABSTRACT					
15. SUBJECT TERMS					
16. SECURITY CLASSIFICATION OF:			17. LIMITATION OF ABSTRACT UU	15. NUMBER OF PAGES	19a. NAME OF RESPONSIBLE PERSON Xiaoning Jiang
a. REPORT UU	b. ABSTRACT UU	c. THIS PAGE UU			19b. TELEPHONE NUMBER 919-515-5240

RPPR Final Report

as of 30-Oct-2017

Agency Code:

Proposal Number: 58405EL

Agreement Number: W911NF-11-1-0516

INVESTIGATOR(S):

Name: Xiaoning Jiang
Email: xjiang5@ncsu.edu
Phone Number: 9195155240
Principal: Y

Name: Fuh-Gwo Yuan
Email: yuan@ncsu.edu
Phone Number: 9195155947
Principal: N

Organization: **North Carolina State University**

Address: 2701 Sullivan Drive, Raleigh, NC 276957514

Country: USA

DUNS Number: 042092122

EIN: 566000756

Report Date: 30-Sep-2017

Date Received: 13-Sep-2017

Final Report for Period Beginning 01-Oct-2011 and Ending 30-Jun-2017

Title: Flexoelectricity in Nanostructures: Theory, Nanofabrication and Characterization

Begin Performance Period: 01-Oct-2011

End Performance Period: 30-Jun-2017

Report Term: 0-Other

Submitted By: Xiaoning Jiang

Email: xjiang5@ncsu.edu

Phone: (919) 515-5240

Distribution Statement: 1-Approved for public release; distribution is unlimited.

STEM Degrees: 0

STEM Participants: 4

Major Goals: The objective of this project is to investigate, theoretically and experimentally, the flexoelectricity at nanometer scale, and explore the feasibility of using flexoelectric micro/nanostructures for novel sensing including seismic, acoustic and IR detections. FE induced effective piezoelectric properties in FE nanostructures could be a few order of magnitudes higher over their conventional bulk materials properties, which will lead to ultrasensitive electromechanical sensors using FE nanostructures. Moreover, flexoelectricity exists in static inhomogeneous deformation. This may mean that electromechanical devices made of FE structures hold the potential of operation over an unprecedented broad bandwidth. The other objective of this research is to understand flexoelectricity of advance flexoelectric (FE) materials in a thermal field where temperature gradient exists. The hypothesis is that when a FE structure is exposed to a thermal field, both direct and converse flexoelectricity can be observed, leading to new electromechanical transduction mechanism. Our recent study on flexoelectrics suggests that FE can be promising for novel electromechanical transduction because of the favorable scaling effect. However, the presence of concurrent electric field gradient and strain/stress gradient in a FE structure has been a challenge, though it is desired to the implementation of flexoelectric structures in many applications. Therefore, the FE-nanostructures can enable ultra-sensitive sensing of environmental parameters at a much broader frequency range as long as these parameters change can induce inhomogeneous strain/stress field. Motivated by recent progress on FE structure and micro/nanofabrication technology, the proposed research efforts will, for the first time, study the flexoelectricity at nanometer scale using a combined theoretical and experimental approach.

Accomplishments: In this report, we investigated the thermal polarization effect where the temperature-dependent dielectric properties of BST were given by the Curie-Weiss law. Derivation of the relationship between the thermal field and the flexoelectricity was accomplished through an analytical model, which was experimentally verified.

Secondly, based on the existence of the converse flexoelectric effect in materials, BST micro/nano-cantilevers with dual comb electrodes were designed and simulated using finite element analysis.

Thirdly, we investigated a new material, BaTiO₃-Bi(Zn_{1/2}Ti_{1/2})O₃ perovskite ceramics (BT-8BZT), at a broad range of temperatures. A fully comparison and analysis were presented in this report.

Furthermore, a metal/ferroelectrics/semiconductor structure was recently tested for its flexoelectricity. The unique direction mechanism were obtained from the experiment.

RPPR Final Report as of 30-Oct-2017

Last but not the least, during the reporting period we also conducted designing new smart materials by alternating its structure. A preliminary model was established for the circular curved microplates, towards smart meta-structures.

Training Opportunities: Two PhD students have been involved in the flexoelectricity study. Two undergraduate students conducted summer intern research together with PhD students.

Results Dissemination: Posters:

Huang, Shujin, Taeyang Kim, Dong Hou, Jacob Jones, and Xiaoning Jiang. "Characterization of the Flexoelectricity in BT-8BZT and its Thermal Dependence." MAE Graduate Research Symposium, Raleigh, NC, 2017.

Huang, Shujin, Taeyang Kim, Dong Hou, Jacob Jones, and Xiaoning Jiang. "Characterization of the Flexoelectricity in BT-8BZT and its Thermal Dependence." Center for Dielectrics & Piezoelectrics 2016 Fall Meeting, Raleigh, NC, Nov. 2016.

Publication:

Huang, S., T. Kim, D. Hou, D. Cann, J. L. Jones, and X. Jiang, "Flexoelectric characterization of BaTiO₃-0.08Bi (Zn_{1/2}Ti_{1/2})O₃", Applied Physics Letters, 110, 22, (2017).

An invited paper is being prepared for the Journal of Advanced Dielectrics.

Honors and Awards: PI received the NC State University Faculty Scholar award.

Protocol Activity Status:

Technology Transfer: Nothing to Report

PARTICIPANTS:

Participant Type: PD/PI

Participant: Xiaoning Jiang PhD

Person Months Worked: 1.00

Project Contribution:

International Collaboration:

International Travel:

National Academy Member: N

Other Collaborators:

Funding Support:

Participant Type: Faculty

Participant: Jiyan Dai

Person Months Worked: 1.00

Project Contribution:

International Collaboration:

International Travel:

National Academy Member: N

Other Collaborators:

Funding Support:

ARTICLES:

RPPR Final Report as of 30-Oct-2017

Publication Type: Journal Article Peer Reviewed: Y **Publication Status:** 1-Published

Journal: Journal of Micromechanics & Microengineering

Publication Identifier Type:

Publication Identifier: doi:10.1088/0960-1317/26/4/045001

Volume: 26

Issue: 0

First Page #: 045001

Date Submitted:

Date Published: 2/22/16 5:00AM

Publication Location:

Article Title: Study on a flexoelectric microphone using barium strontium titanate

Authors: S R Kwon, W B Huang, S J Zhang, F G Yuan, and X Jiang

Keywords: Flexoelectricity, microphone, barium strontium titanate, micro-bridge

Abstract: In this study, a flexoelectric microphone was designed and fabricated in a bridge structure by using barium strontium titanate (Ba_{0.65}Sr_{0.35}TiO₃ or BST) ceramic and tested afterwards. The acoustic test for the prototyped flexoelectric microphone was carried out in an anechoic box with a loud speaker as the acoustic pressure source. The charge sensitivity of the flexoelectric microphone was measured and calculated by compensating the measured charge output with measured acoustic pressure from a reference microphone. The size of the flexoelectric microphone is 1.5 mm × 768 μm × 50 μm in bridge structure. The sensitivity and the resonance frequency were designed to be 0.92 pC/Pa and 98.67 kHz, respectively. In addition, the signal to noise was measured to be 74 dB. The results of experiments exhibit that the flexoelectric microphone possesses high sensitivity and wide working frequency at the same time. It indicates that the flexoelectricity can be an excellent alternative sensing mechanism.

Distribution Statement: 1-Approved for public release; distribution is unlimited.

Acknowledged Federal Support: Y

DISSERTATIONS:

Publication Type: Thesis or Dissertation

Institution:

Date Received: 27-Aug-2015

Completion Date:

Title: Study on Strain Gradient Sensing and Flexoelectric Micro/Nano Structures

Authors:

Acknowledged Federal Support:

Publication Type: Thesis or Dissertation

Institution:

Date Received: 27-Aug-2015

Completion Date:

Title: Flexoelectricity of Barium Strontium Titanate and Its Applications

Authors:

Acknowledged Federal Support:

Flexoelectricity in Nanostructures: Theory, Nanofabrication and Characterization

Technical Final Report (W911 NF-11-1-0516)

Xiaoning Jiang, Shujin Huang, Lu Qi, and Taeyang Kim

Department of Mechanical and Aerospace Engineering
North Carolina State University
Raleigh, NC 27695

Submitted to

Dr. Michael Gerhold
Army Research Office

September 14, 2017

2. Table of Contents

1. Cover page ----- 1

2. Table of contents ----- 2

3. List of illustrations and tables ----- 3

4. Statement of the problem ----- 5

5. Summary of the results ----- 7

6. Bibliography ----- 29

3. List of illustrations and tables

Figure 1. Temperature dependent dielectric permittivity and electric field curves.

Figure 2. The electric field (a) and electric field gradient (b) distribution under 1 V with the temperature of 21 °C at the bottom and 101 °C at the top surface

Figure 3. The experimental setup to measure the thermal gradient induced flexoelectric response.

Figure 4. Schematic of 1D, steady-state heat conduction model (left), analytical graph (right).

Figure 5. Displacement as a function of applying voltages and temperature gradients (a) $L=2$ mm, (b) $L=3$ mm

Figure 6. The temperature-dependent property of the converse flexoelectric coefficient.

Figure 7. The calculated and measured strains of BST samples having different lengths and temperature gradients.

Figure 8. Schematic of dual comb electrodes beam. (Top) Applied electric potential in one unit cell of dual comb electrodes.(Bottom)

Figure 9. The electrical field gradient distribution in x direction.

Figure 10. Schematic of the dual comb electrodes beam (4 unit cells)

Figure 11. The electrical field distribution in x direction.

Figure 12. The electrical field gredients on top (left) and bottom (right).

Figure 13. Schematic view of the experimental set-up.

Figure 14. Plot of the temperature (TC & TM) vs. the cooling time

Figure 15. Plot of μ_{12} of BST and BT-8BZT as a function of temperature.

Figure 16. Temperature dependence of the piezoelectric coefficient d_{33} of BT-8BZT.

Figure 17. Flexoelectric polarization as a function of the applied strain gradient at room temperature. (Pink & red: Pt face up; green & lime: bottom up)

Figure 18. Schematic of a flexoelectric curved circular microplate and its coordinate system

Figure 19. For applied uniform pressure: (a) maximum sensitivity with different ϵ_r ; (b) maximum sensitivity with different f . ($h/l=5$)

Table 1. Dimension of BST samples.

Table 2. Calculated deformation based on different ceramic thickness, electrode width and gap width. (in one unit cell)

Table 3. Geometric parameters of BT-8BZT cantilever beam.

4. Statement of the problem

Flexoelectric effect, defined as a linear coupling effect between a strain gradient and an induced electric polarization [1], has drawn scientific interests in recent years [2]–[14]. This phenomenon is generally expressed in tensor form as [15],

$$\text{Direct : } P_l = \mu_{ijkl} \frac{\partial \varepsilon_{ij}}{\partial x_k} \quad (1)$$

$$\text{Converse : } S_{ij} = f_{ijkl} \frac{\partial E_k}{\partial x_l} \quad (2)$$

where P_l , μ_{ijkl} , ε_{ij} and x_k are the induced polarization, flexoelectric coefficient, elastic strain, and axis of the gradient; S_{ij} , f_{ijkl} and E_k are the strain, converse flexoelectric coefficient associated with strain, and electric field, respectively.

In principle, the flexoelectric effect is a universal phenomenon exhibited by all dielectrics [16]. Consequently, non-piezoelectric materials, such as cubic materials and isotropic materials, still generate electric polarization under an inhomogeneous mechanical field, and yield mechanical strain under an inhomogeneous electric field. In 1964, Kogan first discussed electric polarization in a symmetric crystal by an inhomogeneous deformation, and introduced the concept of flexoelectricity [1]. Experimental and theoretical studies have since confirmed its presence in both crystalline and amorphous dielectrics [17]–[23]. Recently, it has been reported that the scaling effect of direct flexoelectricity has great potential to be an alternative to piezoelectricity for micro/nano devices, suggesting the flexoelectric effect could be more prominent at a micro/nano scale than the piezoelectric effect, even in state-of-the-art piezoelectric materials [2], [24], [25].

Although there have been extensive studies on flexoelectricity under stress and electric field gradients [3], [4], [10], [26], [27], investigations of flexoelectricity under thermal fields have been rather limited. Because of the temperature-dependent dielectric permittivity of flexoelectric materials [28], thermal effects should be a topic of further research. It is expected that a thermal field will induce inhomogeneous dielectric properties inside the flexoelectric materials [29], which will induce the stress/strain gradient under an electric field through a converse flexoelectric effect. Tagantsev investigated a thermal polarization effect in flexoelectricity in the 1980s in which a fundamental relationship between a linear response of the polarization to a temperature gradient was discussed [30], [31]. Tagantsev explained the thermal polarization effect on the flexoelectricity from the concept of a quasi-equilibrium free energy density.

In this report, we investigated the thermal polarization effect where the temperature-dependent dielectric properties of BST were given by the Curie-Weiss law. Derivation of the relationship between the thermal field and the flexoelectricity was accomplished through an analytical model, which was experimentally verified.

Secondly, based on the existence of the converse flexoelectric effect in materials, BST micro/nano-cantilevers with dual comb electrodes were designed and simulated using finite element analysis.

Thirdly, we investigated a new material, $\text{BaTiO}_3\text{--Bi}(\text{Zn}_{1/2}\text{Ti}_{1/2})\text{O}_3$ perovskite ceramics (BT-8BZT), at a broad range of temperatures. A fully comparison and analysis were presented in this report.

Furthermore, a metal/ferroelectrics/semiconductor structure was recently tested for its flexoelectricity. The unique direction mechanism were obtained from the experiment.

Last but not the least, during the reporting period we also conducted designing new smart materials by alternating its structure. A preliminary model was established for the circular curved microplates, towards smart meta-structures.

5. Summary of the results

5.1 Thermal gradient induced flexoelectric effect in bulk $\text{Ba}_{0.67}\text{Sr}_{0.33}\text{TiO}_3$

5.1.1 Theoretical modeling and simulation

Showcased in Fig. 1, a temperature difference along the thickness direction of the material will result in an electric field gradient due to the temperature-dependent dielectric properties of BST. This indicates that strain can be generated following the converse flexoelectric effect. The theoretical analysis of flexoelectricity in a thermal field with a linear distribution can be given by the Curie-Weiss law [15]. The dielectric constant of the ceramics at paraelectric phase is written as

$$\frac{1}{\varepsilon} = \frac{1}{\varepsilon_{\text{peak}}} + \frac{T - T_c}{C} \quad (3)$$

$$T = T_1 + (T_2 - T_1) \frac{x}{L} \quad (4)$$

where ε is the relative dielectric constant, $\varepsilon_{\text{peak}}$ is the peak dielectric constant, T_c is the Curie temperature, C is the Curie-Weiss constant, T_1 and T_2 are the bottom and top temperature of BST, x is the axis, and L is the thickness. For $\text{Ba}_{0.67}\text{Sr}_{0.33}\text{TiO}_3$, $\varepsilon_{\text{peak}} = 18000$, $T_c = 21^\circ\text{C}$, and $C = 1.2 \times 10^5^\circ\text{C}$ [28], [32], [33].

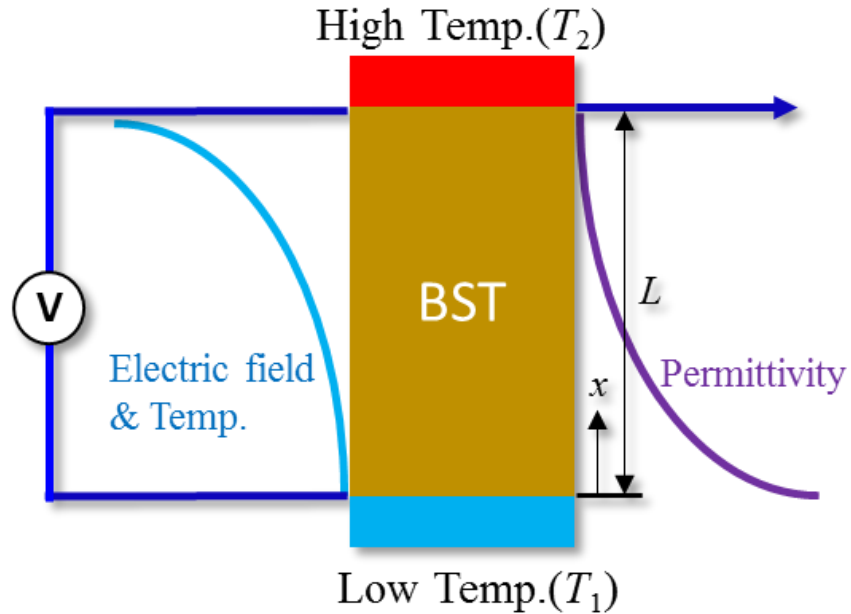


Figure 1. Temperature dependent dielectric permittivity and electric field curves.

The boundary condition requires the electric displacement (D) to be consistent along the height direction, and integration of the electric field equals the total applied voltage (V)

$$\begin{aligned} V &= \int_0^L \left(\frac{1}{\varepsilon_{peak}} + \frac{T_1 + (T_2 - T_1) \frac{x}{L} - T_c}{C} \right) D dx \\ &= \left[\frac{1}{\varepsilon_{peak}} + \frac{1}{2C} \{2(T_1 - T_c) + (T_2 - T_1)\} \right] L \times D \end{aligned} \quad (5)$$

From the above equations, the average electric field gradient ($\frac{\partial E_k}{\partial x_l}$) can then be written as

$$\frac{\partial E_k}{\partial x_l} \cong \frac{E_1 - E_2}{L} = \frac{V}{L^2} \frac{\frac{T_2 - T_1}{C}}{\frac{1}{\varepsilon_{peak}} + \frac{1}{2C} (2(T_1 - T_c) + (T_2 - T_1))} \quad (6)$$

where E_1, E_2 are the electric fields at the bottom and top of BST, respectively.

A finite element analysis was adopted to confirm the above calculations using the COMSOL Multiphysics (COMSOL Inc., Los Angeles, CA). The electric field and electric field gradient distribution are plotted in Fig. 2. The dielectric constant was set to be an expression of the temperature, as depicted by Eq. (3). A 1V voltage drop was applied to the top surface while the bottom surface was set to be ground. A steady state simulation was implemented to obtain the stable temperature distribution and the electric field distribution. Taking into account a 10 mm thickness (L), 21 °C as the bottom surface temperature, and 101 °C as the top surface temperature, an amplitude of the average electric field gradient of 1.714×10^4 V/m² can be observed from the results, supporting the analytical estimation from Eq. (6).

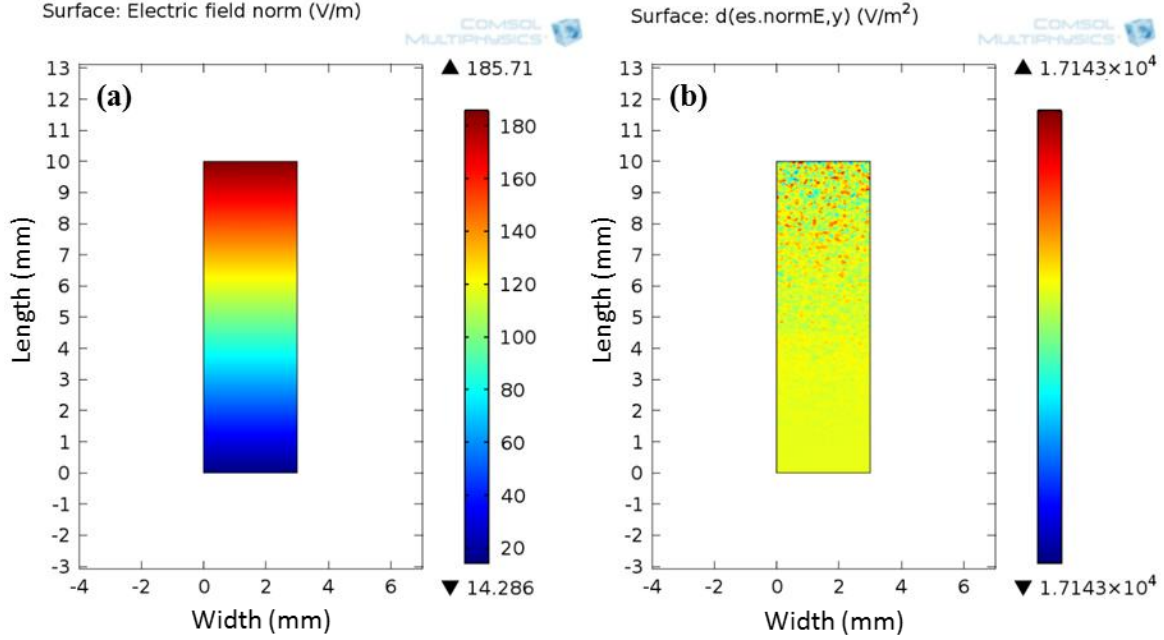


Figure 2. The electric field (a) and electric field gradient (b) distribution under 1 V with the temperature of 21 °C at the bottom and 101 °C at the top surface.

Given a constant temperature difference across the sample surfaces, Eq. (5) yielded that the average electric field gradient is conversely proportional with the square of the thickness L . This unique property implies the great enhancement of the electric field gradient as the structure size shrinks down. Moreover, a great difference in temperature leads to large electric field gradient, which is desired for a converse flexoelectric effect. The converse flexoelectric coefficient of BST is characterized as $f_{1111} = 6 \times 10^{-16} \text{ m}^2/\text{V}$ [9], [34]. The converse flexoelectric effect can be employed here for actuation applications with Eq. (2), where the strain can be readily amplified with a large electric field gradient.

5.1.2 Experimental setup

The experimental setup to measure the thermal gradient-induced flexoelectric response is schematically shown in Fig. 3. The setup was arranged on a floating optical table (Newport, ATS, Irvine, CA) to eliminate vibrational noise. The AC voltage was generated by a power amplifier (Trek, 2220, Lockport, NY) under excitation from a function generator (Tectronix, AFG3101, Lake Mary, FL). To measure the small flexoelectric displacement, the bottom surface of the sample was clamped on the Al rod in which a conductive silver epoxy was adopted as an adhesive and the rigidity of connection was carefully checked out after curing time of silver epoxy. The axial deformation was measured using a high resolution ($<10 \text{ pm}$) laser vibrometer (Polytec, OFV-5000, Irvine, CA) and a lock-in amplifier (Stanford Research System, SR830, Sunnyvale, CA), so the measured displacement was phase-locked with the driving voltage. In

other words, any other background vibration (e.g. building vibration or hot plate vibration if existed) were filtered out and only the flexoelectric vibration was recorded. The applied sinusoidal voltage ranged from 200 V to 1000 V with a frequency of 5 Hz. Heat was applied to BST samples through the heat conductor (Al rod) of a hot plate.

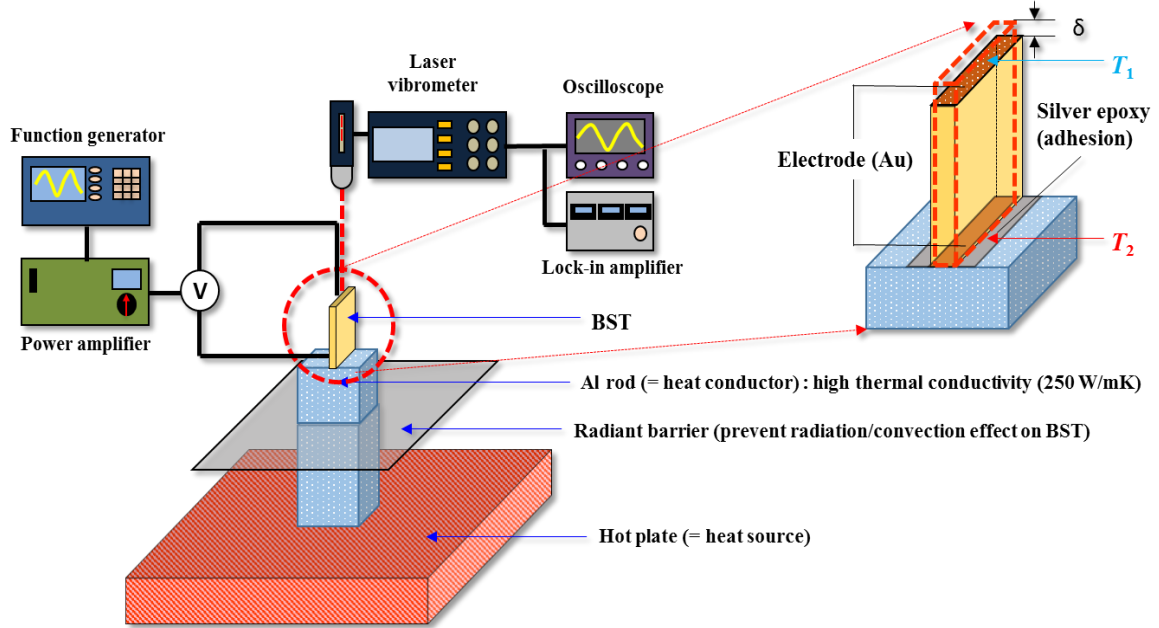


Figure 3. The experimental setup to measure the thermal gradient induced flexoelectric response.

To assure the equilibrium thermodynamic status of BST samples, the temperature of the bottom and top surfaces of the sample was checked every 5 minutes until there was no further temperature change detected. The stabilized temperature difference between the top and bottom of BST samples was measured by a thermocouple (Fluke, 179, Everett, WA) and validated with the 1D, steady-state heat conduction model [35],

$$\frac{T(x) - T_{\infty}}{T_s - T_{\infty}} = \frac{\cosh\{m(L - x)\} + \left(\frac{h}{mk}\right) \sinh\{m(L - x)\}}{\cosh(mL) + \left(\frac{h}{mk}\right) \sinh(mL)}, \quad m^2 = \frac{hP}{kA_c} \quad (7)$$

where T_{∞} , T_s are the ambient and heat source temperature, and L , h , P , k , A_c are the length, convective heat transfer coefficient, plate perimeter, thermal conductivity, and cross-section area of BST samples, respectively. Fig. 4 represents the schematic of 1D, steady-state heat conduction model and the analytical modeling result under the condition ($T_b = 100$ °C, $T_{\infty} = 25$ °C)

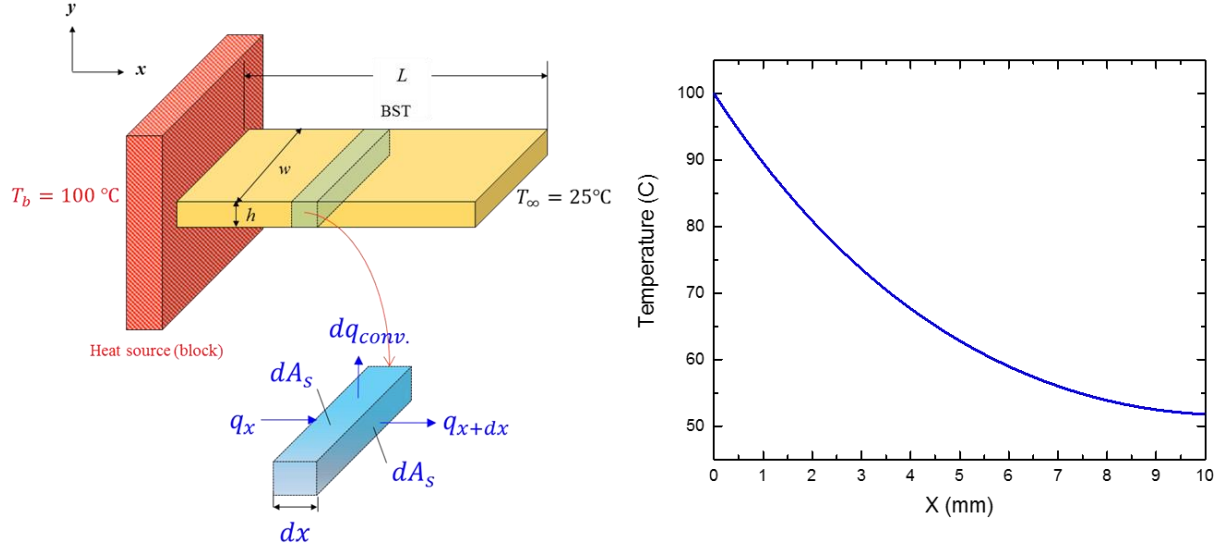


Figure 4. Schematic of 1D, steady-state heat conduction model (left), analytical graph (right).

The electrostrictive effect may contribute to the total displacement, in which the electrostrictive displacement is featured with a higher frequency signal (2ω) than the exciting signal (ω) [26]. Thus, electrostrictive strain can be ruled out by choosing the reference frequency (ω) of the lock-in amplifier to be the same as the exciting signal (ω). Concerning piezoelectricity in BST, when the BST sample temperature is above the Curie temperature ($21\text{ }^{\circ}\text{C}$), the material should theoretically not exhibit any ferroelectricity. Nevertheless, when the temperature is close to the Curie temperature, a weak persistence of the macro-ferroelectric region may exist due to local nano-domains [36]. In Fig. 4, a small displacement ($\sim 2\text{ pm}$) was observed even in the non-thermal gradient condition (room temperature, $23\text{ }^{\circ}\text{C}$), which reflected the residual ferroelectricity. However, compared with the displacement from the thermal gradient-induced flexoelectricity, the piezoelectric contribution to the total displacement can be negligible. As the temperature increases ($> 40\text{ }^{\circ}\text{C}$), this contribution is supposed to be further suppressed.

BST materials used in this work are ceramics fabricated by Texas Instrument as mentioned in Ma's paper²⁸. The fabrication process involves a complex wet chemical route to ensure the local and global homogeneity. Four BST ceramic samples were prepared using dicing and lapping processes, and the dimensions are given in Table I. It is important to note that all the samples were cut from the same BST plate along one direction in order to ensure the homogeneity of the samples. Using the e-beam evaporation, Au was deposited on the top and bottom surfaces of the sample to a 200 nm thickness.

Table 1. Dimension of BST samples.

Sample	Cross-section shape	Dimension ($W_1 \times W_2 \times L$ mm ³)
BST I	Rectangle	$3 \times 0.8 \times \mathbf{3}$
BST II	Rectangle	$2 \times 0.8 \times \mathbf{2}$
BST III	Rectangle	$2 \times 0.8 \times \mathbf{0.2}$
BST IV	Rectangle	$1 \times 0.8 \times \mathbf{0.1}$

5.1.3 Results and discussion

The measured face displacements of samples BST-I and BST-II as a function of the applied voltage and temperature are shown in Figs. 4(a)-(b), respectively. In the tests, the applied voltages ranged from 200 V to 1000 V at 5 Hz, and temperatures at the bottom of BST ranged from 40 °C to 80 °C. Displacement of BST increases directly with the applied voltage, and shows a linear relationship, which is consistent with the analytical expectation. Furthermore, compared with Figs. 4(a) and 4(b), under the same conditions of applied voltage and temperature range, the BST sample with a short length (2 mm) shows a higher displacement than that of the larger BST sample (3 mm), which also well explains the feasibility of the analytical model. It is worth noting that displacement of BST is not proportional to the temperature difference between the top and bottom of the samples, even though the higher temperature difference clearly contributes to the increase of electric field gradient as stated in Eq. (6). This can be elaborated by following Eq. (8),

$$\Delta x = \int_0^L f_{ijkl}(T) \frac{\partial E_k}{\partial x_l} dx \quad (8)$$

Based on Eq. (8), the total displacement of samples was calculated by considering the converse flexoelectric coefficient and the electric field gradient. The converse flexoelectric coefficient, f_{ijkl} , shows the temperature-dependent property. Specifically, f_{ijkl} decreases as the temperature of BST increases above the Curie temperature and finally becomes zero at a certain temperature (~ 101 °C) as shown in Fig. 6 [15],[28],[37]. Therefore, despite the large difference in temperature between the ends of the BST samples, caused by the high temperature applied at the bottom of the BST, further increases the electric field gradient, the converse flexoelectric coefficient decreases at such elevated temperatures, resulting in a decrease in the total displacement of the samples in the end due to overweight of flexoelectric coefficient contribution.

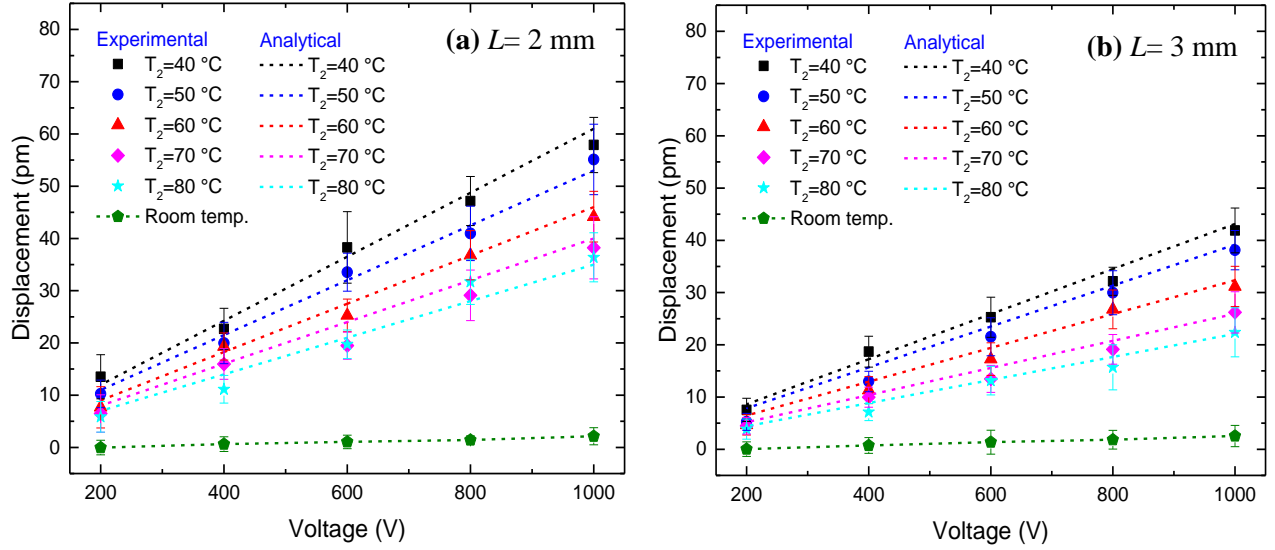


Figure 5. Displacement as a function of applying voltages and temperature gradients
(a) $L=2$ mm, (b) $L=3$ mm

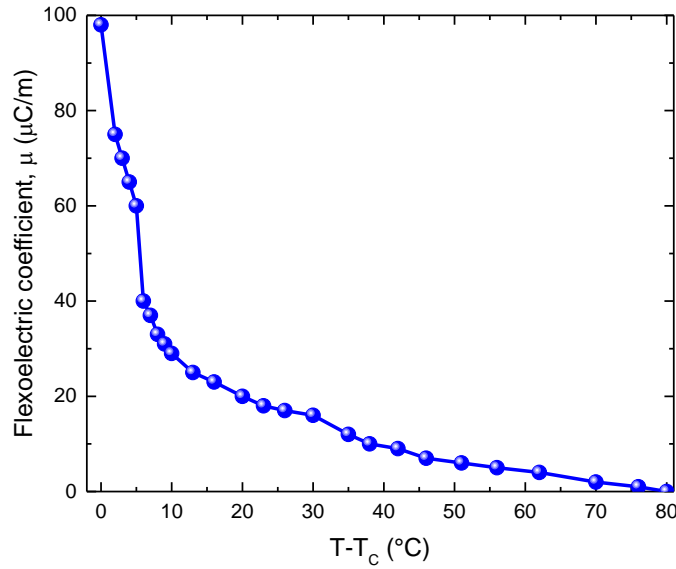


Figure 6. The temperature-dependent property of the converse flexoelectric coefficient.

To further investigate the scaling effect of flexoelectricity, all samples were tested at 400 V and 40 °C bottom temperature. Fig. 7 represents the calculated (based on Eq. (2) and (6)) and measured (based on the measured displacements) strains with different BST samples, in which the smallest sample (BST-IV) shows the highest strain value even in the lowest temperature gradient condition. It also shows that the theoretical analysis is well consistent with the

experimental results on a basis of the trend of data even though there are some discrepancies between them.

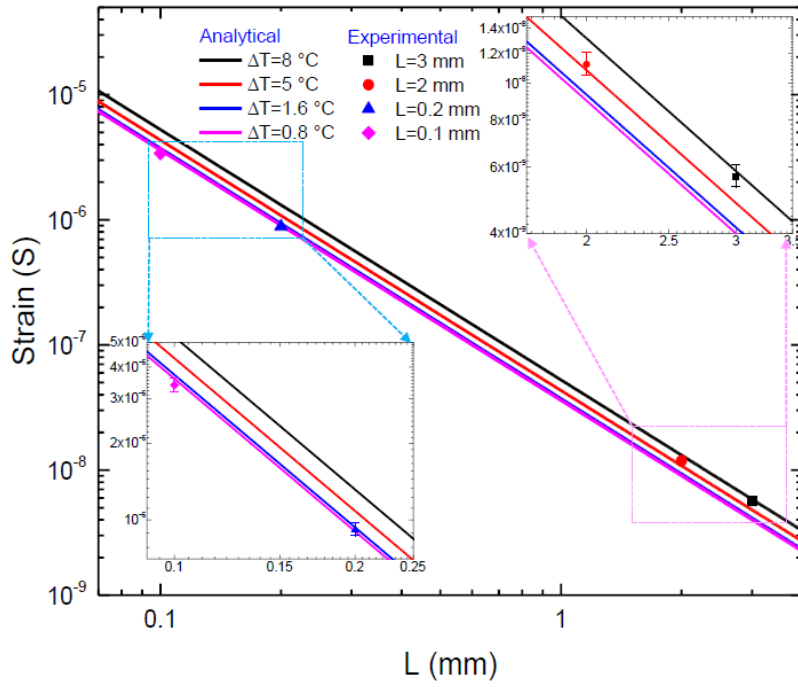


Figure 7. The calculated and measured strains of BST samples having different lengths and temperature gradients.

5.2 Design of flexoelectric nano-cantilevers with dual comb electrodes

5.2.1 Electric field gradient generation

In macro-scaled devices, the electrical potential of parallel electrodes only would generate a perpendicular electrical field distribution. However, in micro-/nano- scale, according to the fringe effect, the electrical potential applied (± 3 V) on one unit cell structure, in Fig. 8, would generate electrical fields both parallel (x direction) and perpendicular (z direction) to the electrode at the edge of nanopatterned electrodes. Due to the non-uniform distribution of these electrical field in the space (within the material), the electric field gradient are generated in both direction.

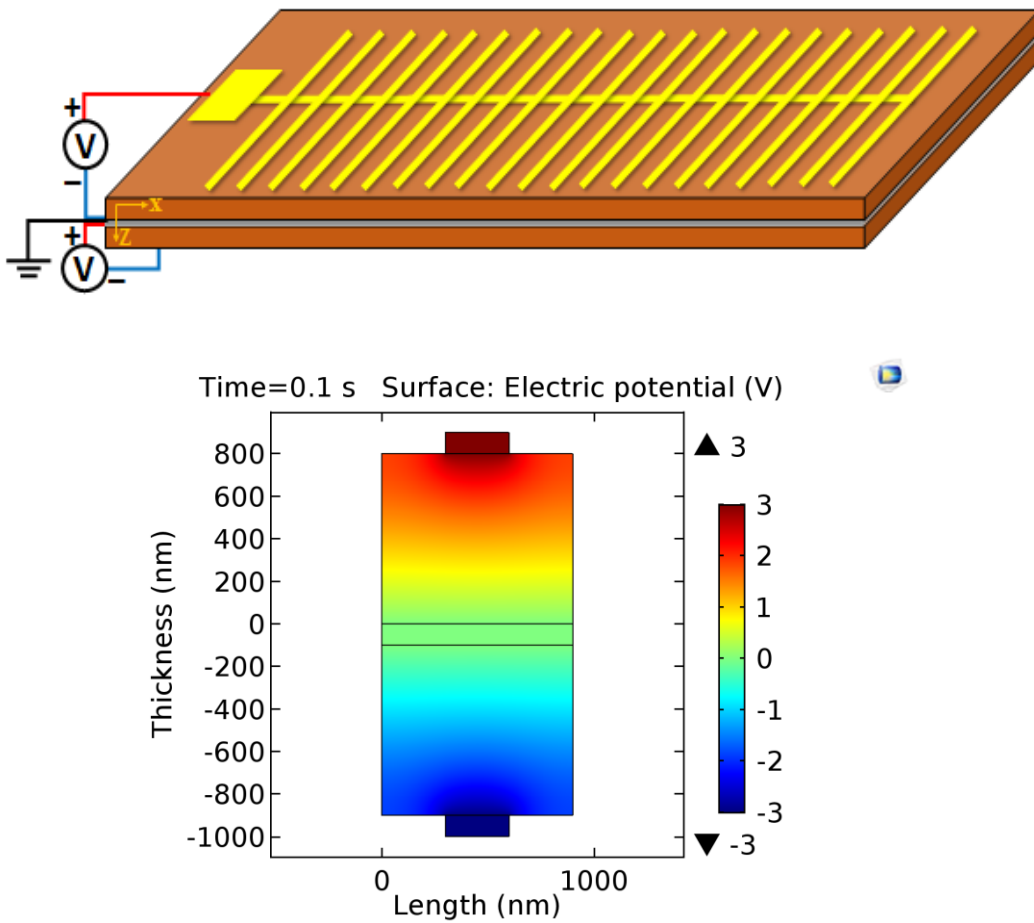


Figure 8. Schematic of dual comb electrodes beam. (Top) Applied electric potential in one unit cell of dual comb electrodes.(Bottom)

The simulation result (COMSOL) in Fig. 9 confirmed the generation of electrical field gradient in x direction.

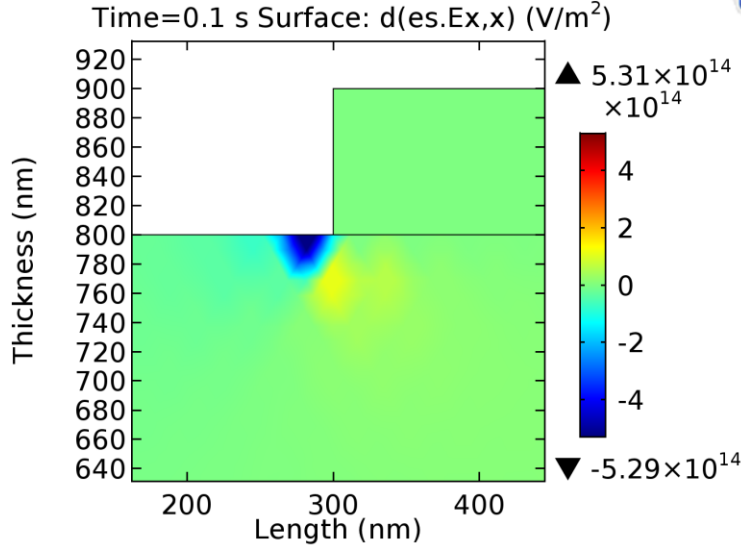


Figure 9. The electrical field gradient distribution in x direction.

According to the conserved flexoelectric effect, a deformation, denoted as S in Eq. (9), would be generated by the electrical field gradient.

$$S = \frac{\mu_{11}}{c_{11}} \frac{\partial E_x}{\partial x} + \frac{\mu_{12}}{c_{11}} \frac{\partial E_z}{\partial z}$$

$$\mu_{11} = 115 [\mu C / m]$$

$$\mu_{12} = 100 [\mu C / m]$$

$$c_{11} = 22.67 \times 10^{10} [N / m^2]$$
(9)

μ_{11} and μ_{12} are the flexoelectric constant, respectively. c_{11} is the elastic stiffness constant. In the case of study, BST is used in further discussion.

5.2.2 Sample design illustration

The schematic of the sample design is illustrated in Fig.10. Both the top and the bottom electrodes of the beam are comb electrodes. The beam is composed by two separate buck BST samples. The insulated ground is at the center layer of the beam, which would provide a protection of the device while applying the electric voltage. Geometrical parameters of the electrodes and the beam are labeled in Fig. 10 as well. Based on the result, other parameters of thickness, electrode width, and electrode gap width have been discussed in the simulation in order to look for an optimized parameter set in further fabrication.

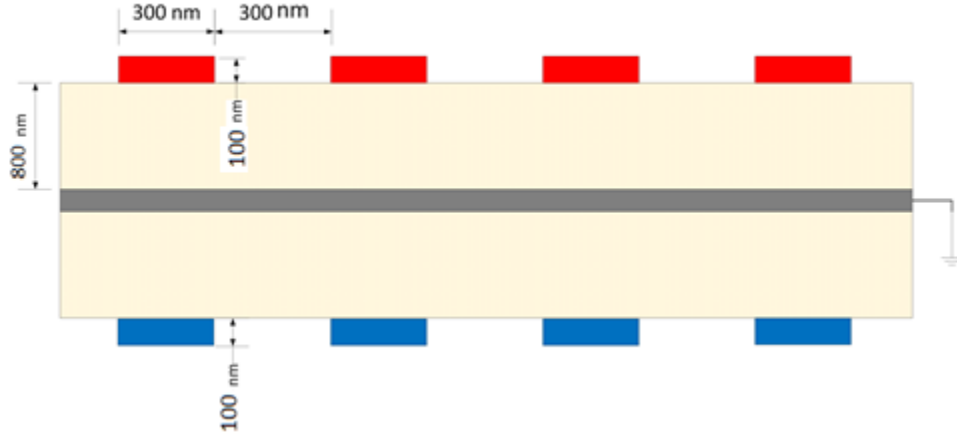


Figure 10. The schematic side view of the dual comb electrodes beam (4 unit cells).

5.2.3 Deformation simulation

A finite element analysis was adopted to confirm the electric field gradients using COMSOL Multiphysics (COMSOL Inc., Los Angeles, CA). The electric field distribution is plotted in Fig. 11. And the electric field gradient distribution on the top surface and the bottom surface are plotted in Fig. 12. The boundary condition was ± 3 V applied voltages on the top and the bottom electrodes. The simulation results show that the electrical field and field gradient are non-uniform in the sample, which agreed with the previous section.

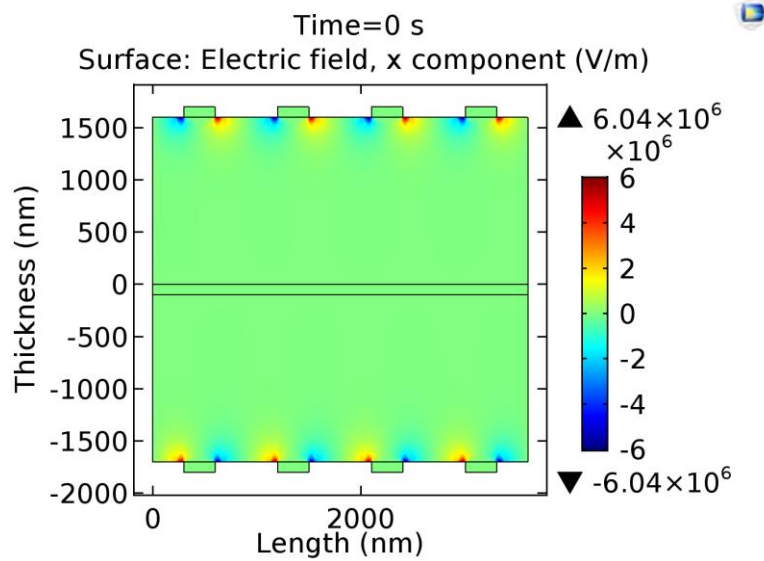


Figure 11. The electrical field distribution in x direction.

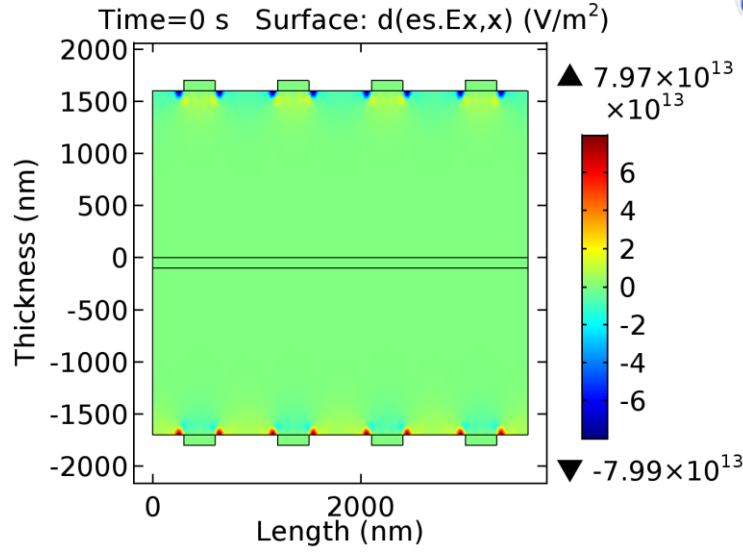


Figure 12. The electrical field gredients distribution in x direction.

Furthermore, based on the simulated value of the electrical field gradient, the deformation of BST can be calculated with Eq. (9). We evaluated 7 different sets of parameters to discuss the trend of increasing the deformation. The top layer contraction and the bottom layer elongation are summarized in Table 2. Then by changing the electrode width, the optimal dimension of the dual comb electrodes can be determined, which would give the largest top contraction and bottom elongation value, listed in Table. 2. Set 1-3 were intended to evaluate the thickness. As the result, thinner ceramic results in larger deformation, which matched the scaling effect of flexoelectric cantilevers [8]. Set 3-5 were intended to evaluate the gap width with constant electrode width. It turned out that the ideal ratio of the electrode width to the gap width would be 1. The fringe effect may vanish when the two electrodes get closer. Set 4, 6 and 7 were evaluating the electrode width with the constant gap width. Narrower the electrode width is, larger the deformation gets. However, in further experimental study, the limitation of fabrication would be critical to select the desired parameter. These evaluation would assist the selection.

Table 2. Calculated deformation based on different ceramic thickness, electrode width and gap width (in one unit cell)

# Set	Ceramic thickness [nm]	Electrode width [nm]	Gap width [nm]	Top contraction [E-4 a.u.]	Bottom elongation [E-4 a.u.]
1	1600	300	600	2.31	2.28
2	800	300	600	6.59	6.57
3	400	300	600	16.75	16.72

4	400	300	300	19.93	19.90
5	400	300	150	18.55	18.42
6	400	30	300	45.79	45.67
7	400	150	300	28.24	28.15

5.3 Thermal dependence of flexoelectricity in BT-8BZT

5.3.1 Experimental processes and results

BT-8BZT ceramics is of interest because of its high permittivity at a broad temperature range. However, the flexoelectricity of BT-8BZT has never been examined. In this study, flexoelectric cantilever beams were fabricated with BT-8BZT and BST ceramics. The dielectric permittivity was examined for BT-8BZT. Then at room temperature, the flexoelectricity of BT-8BZT was measured by using a bending method, while piezoelectricity was directly measured. Furthermore, at different temperatures, the flexoelectric transverse coefficients of BT-8BZT were determined and compared with BST ceramics.

Bulk polycrystalline samples of BT-8BZT ceramics were prepared using a conventional solid state synthesis technique by Cann's research group at Oregon State University, as described in detail by Triamnak et al.¹⁷. The sintered pellets were cut into ceramic bars with an approximate size of $1 \times 5 \times 10 \text{ mm}^3$ using a diamond wire saw (Well Diamond Wire Saws, Inc., Norcross, GA). The cantilever beams of BT-8BZT were prepared using a dicing process. Parameters of the beam are presented in Table 3. Both bottom and top electrodes consist of 100 nm (Au)/5 nm (Ti) prepared by the e-beam evaporation (Kurt Lesker Electron Beam Evaporation System, Jefferson Hills, PA).

Table 3. Geometric parameters of BT-8BZT cantilever beam.

Thickness	Length	Width
780 μm	6.5 mm	4 mm

The cantilever set-up have been discussed in the previous work done by our group [2]. In addition to the room temperature set-up, an extra thermal chamber built with the ceramic fiber blanket is inserted in Fig.13. To record the temperature inside the chamber, both the thermal couple (TC) and the infrared thermal meter (TM) have been used. After 3 minutes of blowing hot air into the chamber by a heat gun, the temperature and the dropping time have been recorded in Fig. 14.

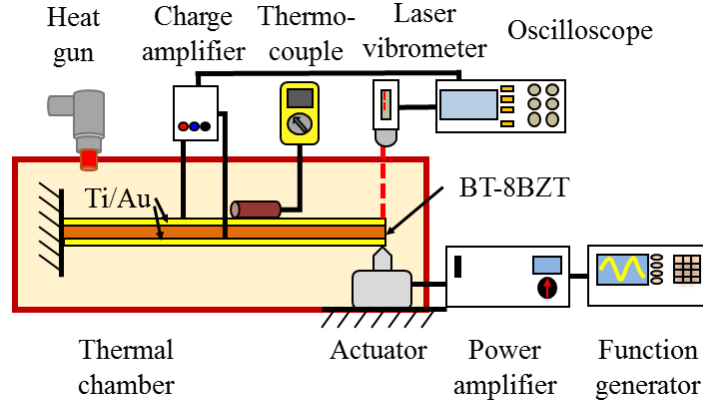


Figure 13. Schematic view of the experimental set-up.

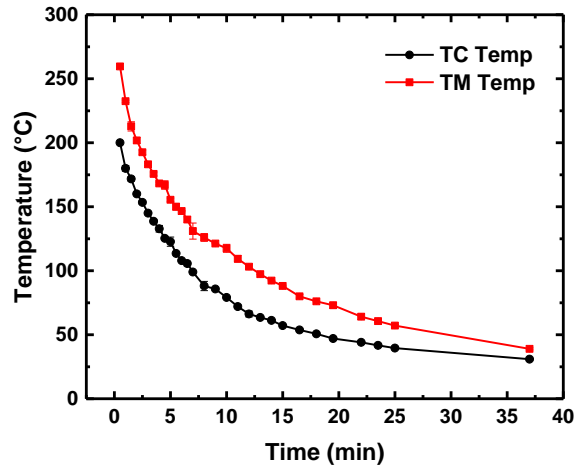


Figure 14. Plot of the temperature (TC & TM) vs. the cooling time.

The thermometer measures the temperature through the infrared radiation, which can be absorbed from everywhere in the insulated environment. This would lead to an accumulation in temperature, which would be higher than the one directly measured by thermocouple. Hence, to simplify the set-up, in the further test, only the thermocouple is used to record the temperature.

Both BST and BT-8BZT cantilever beam had been tested from room temperature to 200 °C. The flexoelectric coefficient is calculated in Eq. (10). I is the current. f is the frequency. δ is the tip displacement. A is the electrode area, L_0 is the cantilever length, x is the distance between the electrode and the clamped end.

$$\mu_{12} = \frac{I \cdot 2\sqrt{2}}{2\pi f \cdot A} \cdot \frac{L_0^2}{3\delta(L_0 - x)} \quad (10)$$

The μ_{12} of BST and BT-8BZT are plotted in Fig. 15. Both BST and BT-8BZT have high flexoelectric coefficients, 25 $\mu\text{C}/\text{m}$ and 22 $\mu\text{C}/\text{m}$ at 25 $^{\circ}\text{C}$, respectively. In BST, an increase in temperature brings the flexoelectricity down rapidly, while the flexoelectric coefficient of BT-8BZT changes more gradually. As the result, the flexoelectric coefficient μ_{12} of BT-8BZT remains around 12 $\mu\text{C}/\text{m}$ at 200 $^{\circ}\text{C}$, while μ_{12} of BST is less than 3 $\mu\text{C}/\text{m}$ at 200 $^{\circ}\text{C}$. Since the temperature range is above the Curie temperature, weak macro-ferroelectric regions may exist due to the presence of local nano-domains which gradually disappear as the temperature is increased. To verify the disappearance of this residual ferroelectricity, the direct piezoelectric response of BT-8BZT was measured over the same temperature range and the data is shown in Fig. 16. As indicated in the figure, the piezoelectric coefficient d_{33} decayed rapidly, which indicates that the piezoelectric effect eventually disappears in the paraelectric phase. Thus, the flexoelectric contribution at high temperatures dominates the mechanical-electrical coupling.

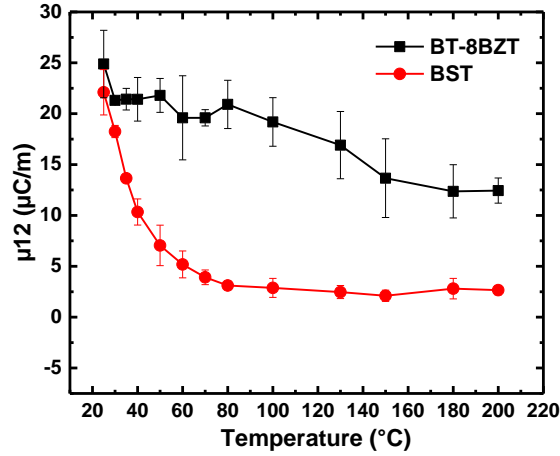


Figure 15. Plot of μ_{12} of BST and BT-8BZT as a function of temperature.

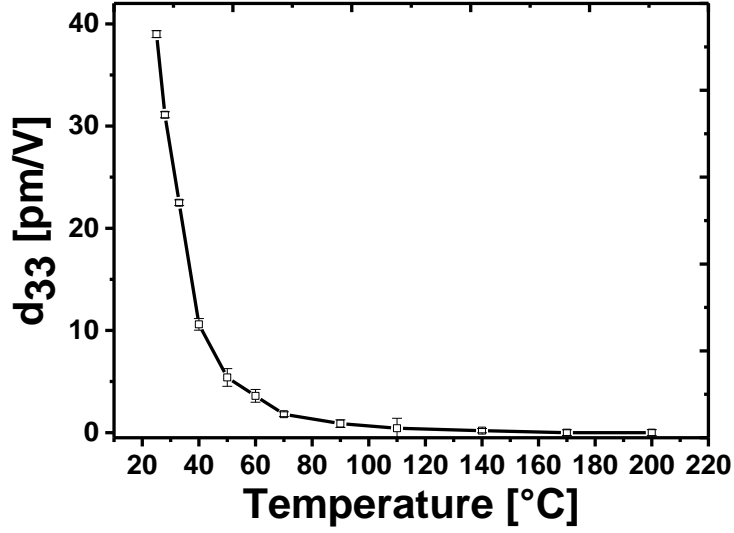


Figure 16. Temperature dependence of the piezoelectric coefficient d_{33} of BT-8BZT.

5.3.2 Discussion

The gradual decline of flexoelectric coefficient μ_{12} with increasing temperature in BT-8BZT was showed in this work, confirming the advantage of a high dielectric permittivity of BT-8BZT in paraelectric phase [38]. The measured flexoelectric coefficient μ_{12} of BT-8BZT is 25 $\mu\text{C}/\text{m}$ at 25 °C and can remain above 12 $\mu\text{C}/\text{m}$ at temperatures up to 200 °C, which suggests potential applications for high temperature micro/nano-sensing. Other compositions in the BiMeO₃-BaTiO₃ system exhibit temperature stable permittivity over a much wider range.²⁴ These findings suggest that these materials may be more effective as flexoelectric-based sensors over a broader temperature range.

5.4 Flexoelectricity in Semiconductor

5.4.1 Theoretical analysis

From the beginning of the study, dielectric insulators have been the objects of flexoelectricity. Recently, semiconductors have been studied for electrical response under a strain gradient. Catalan's group in Spain has demonstrated by doping single crystals of wide-bandgap oxides to increase their conductivity, their effective flexoelectric coefficient was increased by orders of magnitude. Its value is close to 1 mC/m [39]. The samples of BTO- δ are prepared by symmetric annealing. The oxygen depletion process has formed a Schottky barrier at each interfacial barrier layer.

The material we used in this work is Pt/BTO/Nb:STO, where Nb:STO is also an n-type (vacancy) semiconductor. The most fundamental characteristic of rectifying metal-semiconductor junctions, such as Nb:STO, is the Schottky barrier height (SBH), which is the energy discontinuity between the Fermi level of the metal and the conduction band minimum (valence band maximum) of the n-type (p-type) semiconductor. Structures like Pt/BTO/Nb:STO is classified as metal/ferroelectric semiconductor ferroelectric tunnel junctions (FTJs). The resistive switching mechanism appears in such structure with different polarization directions. In our work, the barrier direction would be concerned since it will affect the strain gradient induced electrons flow. The electrical response from bending in different directions will be different due to the different resistivity.

5.4.2 Experimental results

The single-crystalline 0.7wt% Nb-doped SrTiO₃ (Nb:STO) is chosen as the semiconductor substrate. A 100 nm thick BTO film was deposited epitaxially on (001)-oriented Nb:STO substrates by pulsed laser deposition in a typical layer-by-layer growth mode. Pt top electrodes were deposited on BTO/Nb:STO heterostructures to form FTJs. The electrode output were monitored from the Pt electrode and the Nb:STO substrate was always grounded through an indium ohmic contact pad.

Similar experiment set-up was used as described in 5.3, with a temperature control unit. The sample is clamped for one test with Pt electrode being faced up and the other test with the Nb:STO face up, where we aimed to testing how the generated currents are different when the strain gradient is in the same direction.

Fig. 17 shows that the polarization induced by the flexoelectric effect is linearly proportional to the strain gradient, where the slope indicates the average μ_{12} . The effective μ_{12} value for forward direction (Pt face up) is calculated to be $616.93 \pm 74.26 \mu\text{C/m}$ at room temperature, while the effective μ_{12} is $473.45 \pm 34.33 \mu\text{C/m}$ for backward direction (bottom up).

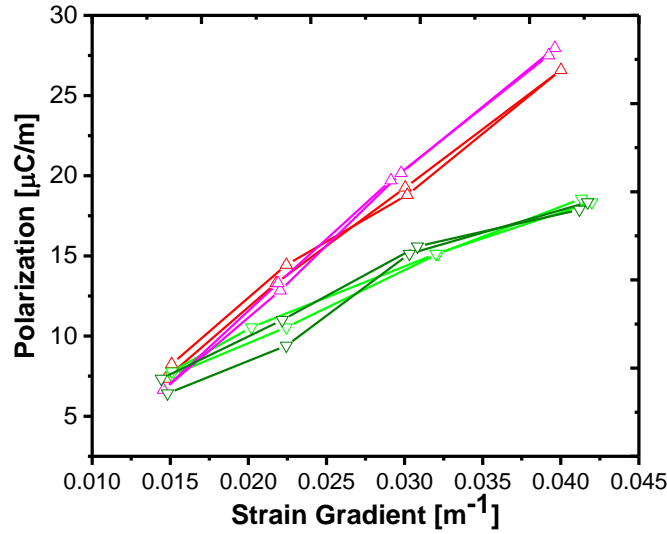


Figure 17. Flexoelectric polarization as a function of the applied strain gradient at room temperature. (Pink & red: Pt face up; green & lime: bottom up)

5.4.3 Discussion

In this work, the flexoelectric switch mechanism is found in Pt/BTO/Nb:STO, which is due to the resistive switch mechanism. The experimental results can support the expectation from the different height at two interfaces of Schottky barriers.

It should be noted that the magnitude of the effect is large comparing with conventional flexoelectricity ($\sim 100 \mu\text{C/m}$). Here we only examined with the one type of semiconductor, transition metal oxides with the perovskite structure. The depletion space charge region on the Nb:STO surface is unique. To draw a further and more thorough conclusion for FTJs structure type, other materials should be studied in the future.

5.5 Flexoelectric metamaterials

5.5.1 Theoretical analysis

The application of flexoelectricity depends on the structure design. The circular microplate structure has become popular in the design of smart material components. Li [40] analyzed the strain gradient elasticity effect on a flexoelectric circular microplate. Furthermore, an enhanced flexoelectricity in curved PZT circular plate was reported by Chu's group [41, 42]. The enhanced magnitude of the mechanical-electrical coupling was claimed due to the inconsistent strain distribution, which is caused by conversion of chemical components during the chemical reduction. In this work, an analytical model was studied to theoretically investigate the

flexoelectric responses in the curved circular plate in order to introduce such materials to sensing and actuating structures.

Based on the flexoelectric theory, a flexoelectric curved circular microplate model is established. The governing equations, boundary conditions and initial conditions are derived following Hamilton's principle.

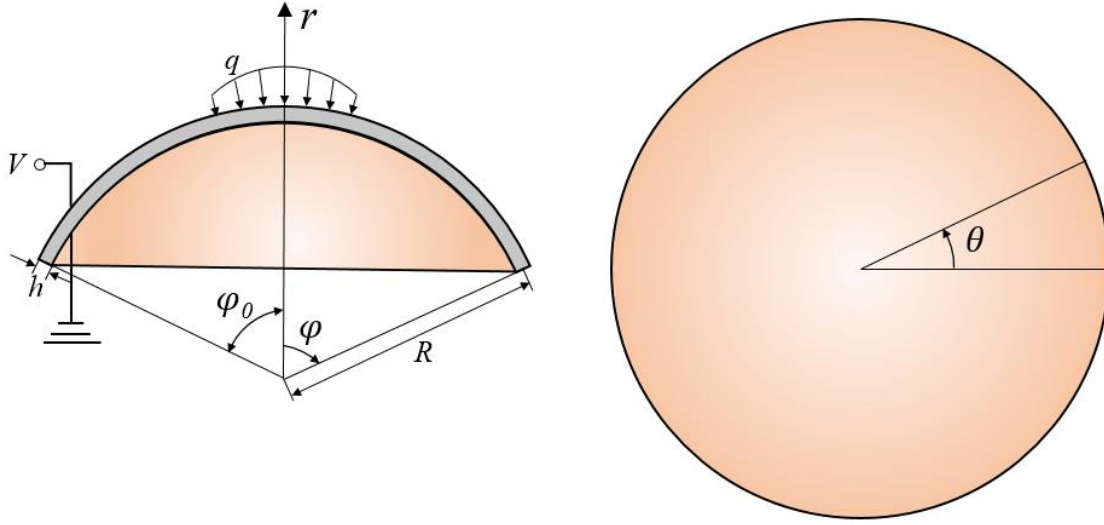


Figure 18. Schematic of a flexoelectric curved circular microplate and its coordinate system

As shown in Fig. 17, the thickness of the curved circular microplate is h . The curvature radius of the central plane is R . The central angle is $2\varphi_0$. The curved circular microplate is subjected to a symmetric distributed force q and a voltage V on the upper surface. A spherical coordinate system is used in the microplate with the $\theta-\varphi$ plane coincident with the central plane and the r -axis along the curvature radius direction. According to the Kirchhoff-Love thin shell theory, the displacement components of the curved circular microplate in the spherical coordinate system are taken as

$$u_r = w(\varphi, t), \quad u_\varphi = \left(\frac{z}{R} + 1 \right) u(\varphi, t) - \frac{z}{R} w_{,\varphi}, \quad u_\theta = 0, \quad (11)$$

Here, $z = r - R$ and u_r , u_φ , u_θ are the displacements in the curvature radius, meridian and latitude direction, respectively. $w(\varphi, t)$, $u(\varphi, t)$ are the deflection and the meridian displacement of central plane, respectively.

Then, we get the flexoelectric-polarization in the direct flexoelectric effect as

$$\begin{aligned}
P_z &= \mu_{1122}(\eta_{\phi\phi r} + \eta_{\theta\theta r}) + 2\mu_{1212}(\eta_{r\phi\phi} + \eta_{r\theta\theta}) = -\frac{1}{R^2}\mu_{1122}\nabla^2 w - \frac{1}{R^2}\mu_{1212}\nabla^2 \tilde{u} - \frac{2}{R^2}(\mu_{1122} + \mu_{1212})w \\
\phi^E &= -\frac{1}{\varepsilon_0} \left[\frac{1}{R^2}\mu_{1122}\nabla^2 w + \frac{1}{R^2}\mu_{1212}\nabla^2 \tilde{u} + \frac{2}{R^2}(\mu_{1122} + \mu_{1212})w \right] \left(z + \frac{h}{2} \right)
\end{aligned} \tag{12}$$

Here, $\eta_{\phi\phi r}, \eta_{\theta\theta r}, \eta_{r\phi\phi}, \eta_{r\theta\theta}$ denote the strain gradients components. μ_{1122}, μ_{1212} are the flexoelectric coefficients, ϕ^E is the electric potential and $\nabla^2 = \frac{\partial^2}{\partial \phi^2} + \cot(\phi) \frac{\partial}{\partial \phi}$.

In the simulation of the direct flexoelectric effect, the induced surface charge linear density is

$$Q(\phi) = 2\pi R \sin(\phi) C^E \phi^E \left(\frac{h}{2} \right), \tag{13}$$

C^E is the capacity per unit surface area defined as $C^E = \varepsilon_r \varepsilon_0 / h$ and ε_r is the dielectric constant.

And hence the total amount of collected charges is

$$Q_{coll} = 2\pi R^2 \int_0^{\phi_0} |Q(\phi)| C^E \sin(\phi) d\phi = \frac{2\pi R^2 \varepsilon_r \varepsilon_0}{h} \int_0^{\phi_0} \left| \phi^E \left(\frac{h}{2} \right) \right| \sin(\phi) d\phi, \tag{14}$$

For the converse flexoelectric effect, the larger deflection is usually the goal. In this case, the applied voltage V is found to be approximately equivalent to an applied uniform pressure $\frac{2(\mu_{1122} + 2\mu_{1212})V}{R^2}$ combined with an applied boundary moment whose linear density is $-\mu_{1122}V$.

To theoretically investigate the flexoelectric responses in the curved circular plate, some numerical simulations and discussions are given. Here, the BST ceramics material is used, whose material parameters are listed in [4]. In the direct flexoelectric effect, $\phi_0 = \pi/10$ and the applied pressure is 0.1MPa. In the converse flexoelectric effect, $h = 1\mu m$ and the applied voltage is 20V. In both cases, $R = 20h / \phi_0$ and the clamped boundary is considered.

In the direct flexoelectric effect, the relation between the bending-induced charge density and the thickness is shown in Figure 19(a). In the converse flexoelectric effect, the relation between the maximum voltage-induced deflection (deflection at the center) and the center angle is shown in Figure 19(b).

5.5.2 Analytical results

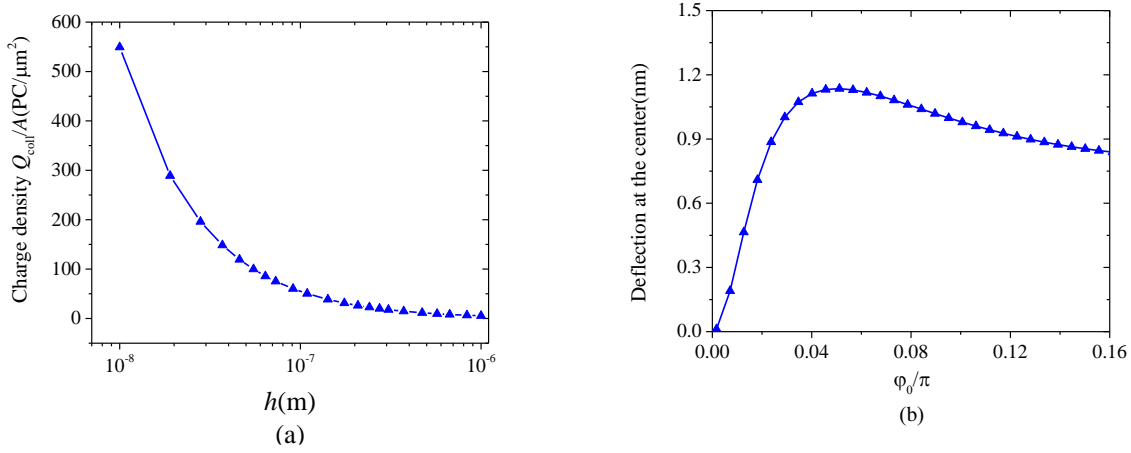


Figure 19. **(a)** Direct flexoelectric effect; **(b)** converse flexoelectric effect

As shown in the Figure 19, in the direct flexoelectric effect, the bending-induced charge-density (A is the surface area) is found significantly increasing as the thickness decreases to nanometer scale, which demonstrates the size-effect of the flexoelectricity in curved circular plate. In the converse flexoelectric response, voltage-induced bending will be generated in the curved plate rather than in the flat circular plate, which demonstrates some advantages for curved circular plate over the flat plate. Here, when the central angle tends to zero, the curved plate gradually turns to be a flat circular plate.

5.5.3 Discussion

The theoretical model of a flexoelectric circular plate is established to calculate its direct and converse flexoelectricity. Based on this theory, we are able to determine the structural sizes according to the target responses. However, the calculated sizes may be only used as reference values since many other factors in the experiment such as fabrication precision, test precision etc. will also affect the results.

5.6 Conclusion

During the final reporting period, the following key results were obtained.

- (1) The flexoelectricity of $Ba_{0.67}Sr_{0.33}TiO_3$ (BST) was investigated by generating temperature gradients along the lengths of samples with symmetric geometry. An electric field gradient induced by a thermal gradient was analyzed based on the temperature-dependent dielectric property of BST. The strain was then experimentally verified due to the electric field gradient. Experimental results suggest converse flexoelectric effect of BST samples with symmetric geometry in a thermal field. This result was not only consistent with the theoretical prediction, but it also followed the scaling effect of flexoelectricity.

- (2) The converse flexoelectric effect was investigated in the BST beam structure. The dual comb electrodes has induced the electrical field gradient and increase the beam deflection. The grounded insulation has simplified the further fabrication work by eliminating the alignment between the top and bottom electrodes.
- (3) The novel material BT-8BZT has been studied for its flexoelectricity. The smooth variation of flexoelectric coefficient has been observed in the experiment in the temperature range from 25 °C to 200 °C. The thermal dependence of flexoelectricity in BT-8BZT can be further adopted in high temperature sensing research.
- (4) The FTJ metal/ferroelectrics/semiconductor structure has been tested for its flexoelectricity. The resistive switch effect not only has a significant in the semiconductor field, but also opens a new direction of design for smart materials in sensing and actuating applications.
- (5) The theoretical model for flexoelectric metamaterials has been derived towards deeper understanding and verification of its intrinsic principle. However, up until now, only a single layered circular curved microplate has been tested under the analytical model. It is still too early to draw a firm conclusion from the current simulation results for layered curved microplates.

References

- [1] S. M. Kogan, “Piezoelectric effect during inhomogeneous deformation and acoustic scattering of carriers in crystals,” *Sov. Phys. Solid State*, vol. 5, pp. 2069–2070, 1964.
- [2] W. Huang, K. Kim, S. Zhang, F.-G. Yuan, and X. Jiang, “Scaling effect of flexoelectric (Ba,Sr)TiO₃ microcantilevers,” *Phys. status solidi - Rapid Res. Lett.*, vol. 5, pp. 350–352, 2011.
- [3] W. Huang, X. Yan, S. R. Kwon, S. Zhang, F. G. Yuan, and X. Jiang, “Flexoelectric strain gradient detection using Ba_{0.64}Sr_{0.36}TiO₃ for sensing,” *Appl. Phys. Lett.*, vol. 101, pp. 0–4, 2012.
- [4] S. R. Kwon, W. B. Huang, S. J. Zhang, F. G. Yuan, and X. N. Jiang, “Flexoelectric sensing using a multilayered barium strontium titanate structure,” *Smart Mater. Struct.*, vol. 22, p. 115017, 2013.
- [5] X. Jiang, W. Huang, and S. Zhang, “Flexoelectric nano-generator: Materials, structures and devices,” *Nano Energy*, vol. 2, pp. 1079–1092, 2013.
- [6] W. Huang, S.-R. Kwon, S. Zhang, F.-G. Yuan, and X. Jiang, “A trapezoidal flexoelectric accelerometer,” *J. Intell. Mater. Syst. Struct.*, vol. 25, pp. 271–277, 2013.
- [7] X. Yan, W. Huang, S. Ryung Kwon, S. Yang, X. Jiang, and F.-G. Yuan, “A sensor for the direct measurement of curvature based on flexoelectricity,” *Smart Mater. Struct.*, vol. 22, p. 085016, 2013.
- [8] Y. Li, L. Shu, W. Huang, X. Jiang, and H. Wang, “Giant flexoelectricity in Ba_{0.6}Sr_{0.4}TiO₃/Ni_{0.8}Zn_{0.2}Fe₂O₄ composite,” *Appl. Phys. Lett.*, vol. 105, p. 162906, 2014.
- [9] L. Shu, W. Huang, S. Ryung Kwon, Z. Wang, F. Li, X. Wei, S. Zhang, M. Lanagan, X. Yao, and X. Jiang, “Converse flexoelectric coefficient f_{1212} in bulk Ba_{0.67}Sr_{0.33}TiO₃,” *Appl. Phys. Lett.*, vol. 104, p. 232902, 2014.
- [10] L. Shu, F. Li, W. Huang, X. Wei, X. Yao, and X. Jiang, “Relationship between direct and converse flexoelectric coefficients,” *J. Appl. Phys.*, vol. 116, p. 144105, 2014.
- [11] S. R. Kwon, W. Huang, L. Shu, F.-G. Yuan, J.-P. Maria, and X. Jiang, “Flexoelectricity in barium strontium titanate thin film,” *Appl. Phys. Lett.*, vol. 105, p. 142904, 2014.
- [12] W. Huang, S. Yang, N. Zhang, F.-G. Yuan, and X. Jiang, “Direct Measurement of Opening Mode Stress Intensity Factors Using Flexoelectric Strain Gradient Sensors,” *Exp. Mech.*, vol. 55, pp. 313–320, 2015.

- [13] U. K. Bhaskar, N. Banerjee, A. Abdollahi, Z. Wang, D. G. Schlom, G. Rijnders, and G. Catalan, “A flexoelectric microelectromechanical system on silicon,” *Nat. Nanotechnol.*, no. November, pp. 2–6, 2015.
- [14] U. K. Bhaskar, N. Banerjee, A. Abdollahi, G. Rijnders, E. Solanas, and G. Catalan, “Flexoelectric MEMS: towards an electromechanical strain diode,” *Nanoscale*, 2015.
- [15] L. E. Cross, “Flexoelectric effects: Charge separation in insulating solids subjected to elastic strain gradients,” *J. Mater. Sci.*, vol. 41, pp. 53–63, 2006.
- [16] H. Le Quang and Q.-C. He, “The number and types of all possible rotational symmetries for flexoelectric tensors,” *Proc. R. Soc. A Math. Phys. Eng. Sci.*, vol. 467, pp. 2369–2386, 2011.
- [17] W. Ma and L. E. Cross, “Large flexoelectric polarization in ceramic lead magnesium niobate,” *Appl. Phys. Lett.*, vol. 79, pp. 4420–4422, 2001.
- [18] W. Ma and L. E. Cross, “Flexoelectric effect in ceramic lead zirconate titanate,” *Appl. Phys. Lett.*, vol. 86, pp. 1–3, 2005.
- [19] W. Ma and L. E. Cross, “Flexoelectricity of barium titanate,” *Appl. Phys. Lett.*, vol. 88, p. 232902, 2006.
- [20] Z. Wang, X. X. Zhang, X. Wang, W. Yue, J. Li, J. Miao, and W. Zhu, “Giant flexoelectric polarization in a micromachined ferroelectric diaphragm,” *Adv. Funct. Mater.*, vol. 23, pp. 124–132, 2013.
- [21] S. Baskaran, X. He, Q. Chen, and J. Y. Fu, “Experimental studies on the direct flexoelectric effect in α -phase polyvinylidene fluoride films,” *Appl. Phys. Lett.*, vol. 98, p. 242901, 2011.
- [22] J. Narvaez and G. Catalan, “Origin of the enhanced flexoelectricity of relaxor ferroelectrics,” *Appl. Phys. Lett.*, vol. 104, pp. 78–82, 2014.
- [23] P. Zubko, G. Catalan, and A. K. Tagantsev, “Flexoelectric Effect in Solids,” *Annu. Rev. Mater. Res.*, vol. 43, pp. 387–421, 2013.
- [24] M. S. Majdoub, P. Sharma, and T. Cagin, “Enhanced size-dependent piezoelectricity and elasticity in nanostructures due to the flexoelectric effect,” *Phys. Rev. B - Condens. Matter Mater. Phys.*, vol. 77, p. 125424, 2008.
- [25] J. Y. Fu, W. Zhu, N. Li, N. B. Smith, and L. Eric Cross, “Gradient scaling phenomenon in microsize flexoelectric piezoelectric composites,” *Appl. Phys. Lett.*, vol. 91, no. 2007, p. 182910, 2007.

- [26] W. Huang, L. Shu, S. R. Kwon, and S. Zhang, "Fabrication and measurement of a flexoelectric micro-pyramid composite," *AIP Adv.*, vol. 4, p. 127115, 2014.
- [27] L. M. Garten and S. Trolier-McKinstry, "The field induced e_{31} , f piezoelectric and Rayleigh response in barium strontium titanate thin films," *Appl. Phys. Lett.*, vol. 105, p. 132905, 2014.
- [28] W. Ma and L. E. Cross, "Flexoelectric polarization of barium strontium titanate in the paraelectric state," *Appl. Phys. Lett.*, vol. 81, pp. 3440–3442, 2002.
- [29] A. Biancoli, C. M. Fancher, J. L. Jones, and D. Damjanovic, "Breaking of macroscopic centric symmetry in paraelectric phases of ferroelectric materials and implications for flexoelectricity," *Nat. Mater.*, vol. 14, pp. 224–229, 2014.
- [30] A. K. Tagantsev, "Pyroelectric , piezoelectric , flexoelectric , and thermal polarization effects in ionic crystals Pyroelectric , piezoelectric , flexoelectric , and thermal polarization effects in ionic crystals," *Sov. Phys. Uspekhi*, vol. 30, pp. 588–603, 1987.
- [31] A. K. Tagantsev, "Electric polarization in crystals and its response to thermal and elastic perturbations," *Phase Transitions*, vol. 35, pp. 119–203, 1991.
- [32] C. Fu, C. Yang, H. Chen, Y. Wang, and L. Hu, "Microstructure and dielectric properties of $\text{Ba}_{1-x}\text{Sr}_x\text{TiO}_3$ ceramics," *Mater. Sci. Eng. B*, vol. 119, pp. 185–188, 2005.
- [33] S. Lahiry and a. Mansingh, "Dielectric properties of sol-gel derived barium strontium titanate thin films," *Thin Solid Films*, vol. 516, pp. 1656–1662, 2008.
- [34] J. Y. Fu, W. Zhu, N. Li, and L. E. Cross, "Experimental studies of the converse flexoelectric effect induced by inhomogeneous electric field in a barium strontium titanate composition," *J. Appl. Phys.*, vol. 100, p. 024112, 2006.
- [35] T. L. Bergman, A. S. Lavine, F. P. Incropera, and D. P. Dewitt, *Fundamentals of heat and mass transfer*, 7th ed. Wiley, 2011, p. 159.
- [36] M. Roth, E. Mojaev, E. Dul'kin, P. Gemeiner, and B. Dkhil, "Phase transition at a nanometer scale detected by acoustic emission within the cubic phase $\text{Pb}(\text{Zn}_{1/3}\text{Nb}_{2/3})\text{O}_3$ - $x\text{PbTiO}_3$ relaxor ferroelectrics," *Phys. Rev. Lett.*, vol. 98, p. 265701, 2007.
- [37] L. M. Garten and S. Trolier-McKinstry, "Enhanced flexoelectricity through residual ferroelectricity in barium strontium titanate," *J. Appl. Phys.*, vol. 117, p. 094102, 2015.
- [38] Triamnak, Narit, et al. "Phase formation of BaTiO_3 - $\text{Bi}(\text{Zn}_{1/2}\text{Ti}_{1/2})\text{O}_3$ perovskite ceramics." *Journal of the Ceramic Society of Japan*, vol.122(1424), pp. 260-266, 2014.

- [39] Narvaez, Jackeline, Fabian Vasquez-Sancho, and Gustau Catalan. "Enhanced flexoelectric-like response in oxide semiconductors." *Nature* 538.7624 (2016): 219-221.
- [40] Li A, Zhou S, Qi L. "Size-dependent electromechanical coupling behaviors of circular micro-plate due to flexoelectricity." *Applied Physics A*, 2016, 122(10): 918.
- [41] Zhou W, Chen P, Pan Q, et al. "Lead - Free Metamaterials with Enormous Apparent Piezoelectric Response." *Advanced Materials*, 2015, 27(41): 6349-6355.
- [42] Zhou W, Chu B. "Strong Electromechanical Response in Lead Zirconate Titanate Metamaterials." *Journal of the American Ceramic Society*, 2016, 99(10): 3317-3324.